Sixth International Symposium on Turbulence and Shear Flow Phenomena
Seoul, Korea, 22-24 June 2009

SPATIO-TEMPORALLY PERIODIC CONTROL FOR TURBULENT FRICTION DRAG REDUCTION

Aiko YAKENO, Yosuke HASEGAWA and Nobuhide KASAGI
Department of Mechanical Engineering
The University of Tokyo
Hongo 7-3-1, Bunkyo-ku, Tokyo 113-8656, Japan
yakeno@thtlab.t.u-tokyo.ac.jp

ABSTRACT

We evaluate the temporally- and spatially-periodic spanwise pre-determined control. The spatially-periodic control achieves better performance than the temporally-periodic control, which is conventional spanwise wall-oscillation control. To analyze the drag reducing mechanisms, we focus on the near-wall structure, a longitudinal vortex and a low-speed streak. Then we assume that the drag is reduced by positional change of the vortex and the low-speed streak.

INTRODUCTION

Background and Objectives

Turbulence control should have a huge impact on reduction of energy consumption. For example, the turbulent friction drag accounts for about a half of total energy consumed by an aircraft (Filippone, 2000).

Compared with passive control, active control has a higher potential to manipulate turbulent flows flexibly and robustly. Among them, predetermined control recently attracts much attention because it does not need massively arrayed miniature sensors and actuators, which are required by feedback control. Recently, some spatio-temporally predetermined controls have been proposed, e.g., spanwise wall-oscillation control (Jung *et al*., 1992), local temporally-periodic blowing (Tardu, 1998), spanwise / streamwise traveling wave control (Du and Karniadakis, 2000; Min *et al*., 2006). Among them, spanwise control inputs are more affective than other directions and some research has been focused on. Although, the details of drag reduction mechanisms have not been fully understood.

General expression of these spanwise control inputs are given by:

$$w_{wall}(x,z,t) = W_0 \cdot \mathrm{Real}\left[\exp\left\{i\left(\omega t + k_x x + k_z z\right)\right\}\right] \quad (1)$$

Here, $\omega = 2\pi/T$, $k_x = 2\pi/\lambda_x$ and $k_z = 2\pi/\lambda_z$, where T, λ_x and λ_z are a time period and wavelengths in the streamwise and spanwise direction, respectively. Obviously, when $\omega \neq 0$ and $k_x = k_z = 0$, Eq. (1) corresponds to the conventional wall-oscillation control. In this paper, we refer to it as the temporally-periodic control.

These above-mentioned predetermined controls commonly suffer from large power input although they generally achieve considerable drag reduction. The temporally-periodic control achieve friction drag reduction of over 45%, while the highest energy saving rate, be discussed below, is at the most 7%, when the oscillation period is $T^+ = 125$ and the amplitude is $W_0^+ = 4.5$ (Quadrio and Ricco, 2004). Here, the variable with superscript of + represents a value in the wall units. Hence, one of major issues is to develop a new control scheme that brings large drag reduction rate with less power input. Recently, a new control input, which is stationary, but longitudinally-periodic, has been just proposed, and this was found to be more effective in terms of net energy saving than the conventional temporally-periodic control. This control input corresponds to the case that $k_x \neq 0$ and $\omega = k_z = 0$ in Eq. (1) (as shown in Fig. 1). We call it as a spatially-periodic control.

In this paper, we focus on the temporally- and spatially-periodic controls. By systematically changing the temporal period and the wavelength of the control input, we evaluate the two control schemes in terms of net energy saving, and discuss the optimal periodicity in the two controls. Finally, we discuss drag reduction mechanisms of the two control algorisms on the bases of the near-wall structure.

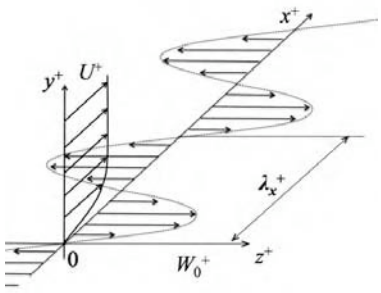

Fig. 1 Schematic of spatially-periodic input at the wall.

Performance Indices for Control

We consider a fully developed turbulent channel flow driven by a pressure gradient under a constant mass flow rate.

Pumping power P is defined with the channel half-width δ as:

$$P = \int_0^{2\delta} \left(-\overline{u}(y)\frac{\partial \overline{p}}{\partial x}\right) dy. \quad (2)$$

The instantaneous power input for spanwise wall motion w_{wall} is given by:

$$P_{in} = \frac{1}{L_x}\frac{1}{L_z}\int_{L_x}\int_{L_z}\left(w_{wall}\left.\frac{\partial w}{\partial y}\right|_{y=0}\right)dxdz. \quad (3)$$

Here, L_x and L_z are the control surface dimensions in the streamwise and spanwise directions, respectively, and y is the distance from the wall.

In order to evaluate a control scheme, we focus on the following three quantities, i.e., drag reduction rate, gain and energy saving rate.

Drag Reduction Rate: the reduction rate of the friction drag coefficient C_f relative to that in the uncontrolled flow.

$$DR = \left(C_{f0} - C_f\right)/C_{f0}. \quad (4)$$

A variable with subscript of 0 represents a quantity in the uncontrolled case.

Gain: the reduction of pumping power input divided by power input.

$$G = \left(P_0 - P\right)/P_{in}. \quad (5)$$

Energy Saving Rate: the reduction of total power input ($P + P_{in}$), divided by the pumping power in the uncontrolled flow.

$$S = \left(P_0 - P - P_{in}\right)/P_0. \quad (6)$$

COMPUTATIONAL METHODS

Governing equations are the incompressible Navier-Stokes and continuity equations. We use a periodic boundary condition in the streamwise and spanwise directions, and a no-slip condition at the two walls. A central finite-difference method is adopted for spatial discretization with second-order of accuracy. The second order Adams-Bashforth method is used for convection terms, while the Crank-Nicolson method for viscous terms. A fractional step method is applied to decouple pressure from the Navier-Stokes equation.

All simulations are performed under a constant streamwise flow rate U_b unless otherwise stated. The bulk Reynolds number based on U_b and the channel half-width δ is $\mathrm{Re}_b = 2228$, which corresponds to the friction Reynolds number $\mathrm{Re}_\tau = 150$ in the uncontrolled case. The computational domain is $2.5\pi\delta \times 2\delta \times \pi\delta$, in the streamwise, wall-normal and spanwise directions. The number of grids is $(N_x, N_y, N_z) = (64, 128, 64)$, while the spatial resolutions are $\Delta x^+ = 18.4$, $\Delta y^+ = 0.189 \sim 5.70$ and $\Delta z^+ = 7.36$. In the case of spatially-periodic control, the streamwise domain is extended in accordance with the streamwise wavelength of the control input ($L_x = 2.5\pi\delta \sim 4\pi\delta$, $\Delta x^+ = 9.20 \sim 18.4$). As for the control input, variable parameters in the temporally-periodic control are the amplitude W_0^+ and the oscillation period T^+ while W_0^+ and the streamwise wavelength λ_x^+ in spatically-periodic control. 256 computations are run for each control scheme in order to systematically change the above two parameters.

CONTROL EFFECT

Fig. 2 (a) and (b) show obtained drag reduction rate in temporally- and spatially-periodic controls. In both figures, the vertical axis in the amplitude W_0^+. The horizontal axes in Fig. 1 (a) and (b) are the temporal period T^+ and the wavelength λ_x^+. In both controls, DR increases with increasing W_0^+. There exist the optimal time period of $T^+ \sim 100$ and wavelength of $\lambda_x^+ \sim 1000$ in temporally- and spatially-periodic controls, respectively. In general, the spatially-periodic control achieves higher DR than the temporally-periodic control. Fig. 3 and 4 show comparison between two controls in terms of the gain G and the energy saving rate S. The spatially-periodic control gives higher G and S than temporally-periodic control. From these results, we conclude that spatially-periodic control is superior in terms of both the gain G and the energy saving rate S.

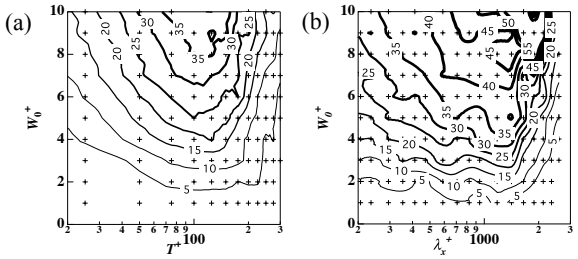

Fig. 2 DR ×100 (%) as a function of time period, wavelength and amplitude. (a) temporally-periodic control, (b) spatially-periodic control.

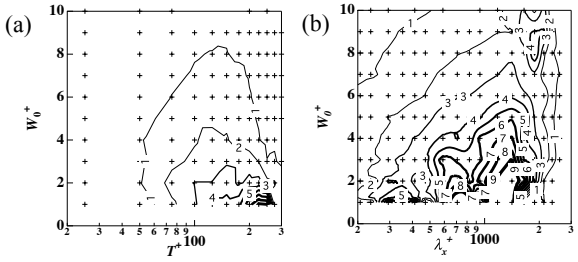

Fig. 3 G as a function of time period, wavelength and amplitude. (a) temporally-periodic control, (b) spatially-periodic control.

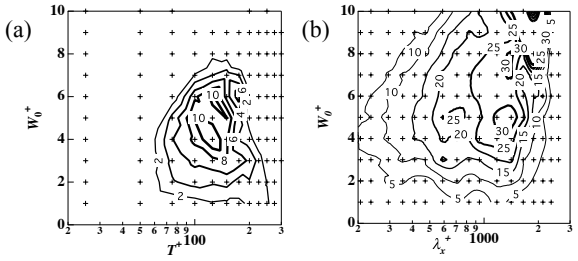

Fig. 4 S ×100 (%) as a function of time period, wavelength and amplitude. (a) temporally-periodic control, (b) spatially-periodic control.

Fig. 5 shows a time traces of pumping power input P_{in} temporally- and spatially-periodic controls when $T^+ = 125$ and $\lambda_x^+ = 1178$, respectively. The amplitude is set to be $W_0^+ = 7.0$ in both cases. Comparing the two controls, time-averaged power input is almost the same, while the

friction drag is more reduced in the spatially-periodic control. This explains why higher net energy saving rate is achieved in the spatially-periodic control as shown in Fig. 4.

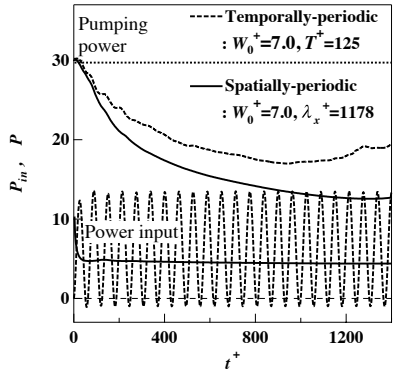

Fig. 5 Time traces of energy balance, pumping power decreasing and control power input.

To interpret the physical meaning of the optimum wavelength in the spatially-periodic control, we introduce a new coordinates system that moves with a typical convection velocity $u_c^+ \sim 10$ at $y^+ \sim 15$, where the longitudinal vortices are likely exist. Then we convert the spatial periodicity into the temporal periodicity by using following relationship:

$$T_c^+ = \frac{\lambda_x^+}{u_c^+}. \tag{7}$$

Assuming $\lambda_x^+ = 1000$, the converted temporal period of the spatially-periodic control is $T_c^+ \sim 100$, which agree with the optimum period of the temporally-periodic control. It is known that the dynamics of coherent structures have a periodical generation-destruction cycle (Jimenez and Moin, 1991; Kawahara and Kida, 2001). The present results suggest that the spanwise fluctuation of this particular frequency at the position of $y^+ \sim 15$ is effective to diminish the active coherent structures near the wall.

MECHANISMS OF DRAG REDUCTION

Phase Analysis

To explore the mechanisms of drag reduction in temporally- and spatially-periodic controls, we coordinated additional computations with the optimal temporal period of $T^+ = 125$, and the wavelength $\lambda_x^+ = 1178$, respectively. In both computations, the amplitude is set to be $W_0^+ = 7.0$. These are run under a constant pressure gradient in order to keep the wall shear stress constant and therefore minimize the Reynolds number effects.

When a periodic control is imposed, the resultant velocity field can be considered as a superposition of periodic and irregular fluctuations. Therefore, the instantaneous velocity u_i, can be decomposed into a spatio-temporal mean component $\overline{u}_i$, phase fluctuation component $\tilde{u}_i$, and a random incoherent component u_i'':

$$u_i = \overline{u}_i + \tilde{u}_i + u_i''. \tag{8}$$

A phase-averaged quantity is given by:

$$\overline{u}_i + \tilde{u}_i = \langle u_i \rangle_\phi = \lim_{N\to\infty} \frac{1}{N} \sum_{n=0}^{N} u_i(\phi). \tag{9}$$

Fig. 6 ~ 8 show the phase fluctuation parts of each velocity component. (a) is temporally-periodic control, (b) is spatially-periodic control. It is found that $\tilde{u}$ and $\tilde{v}$ are much smaller than that of $\tilde{w}$. It should be noted that $\tilde{v}$ in the temporally-periodic control is analytically zero due to the continuity equation. In additional, the temporal or spatial oscillation period of $\tilde{u}$ and $\tilde{v}$ is a half of that of $\tilde{w}$. This is due to symmetric property of the present flow configuration in the spanwise direction.

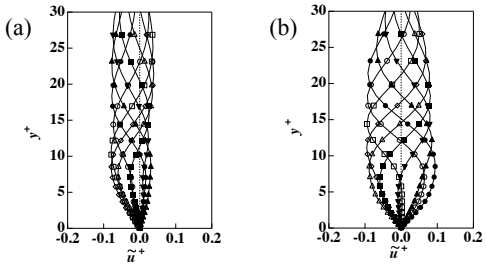

Fig. 6 Phase fluctuation parts of $\tilde{u}$. (a) temporally-periodic control, (b) spatially-periodic control.

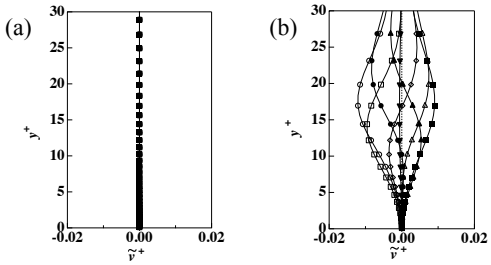

Fig. 7 Phase fluctuation parts of $\tilde{v}$. (a) temporally-periodic control, (b) spatially-periodic control.

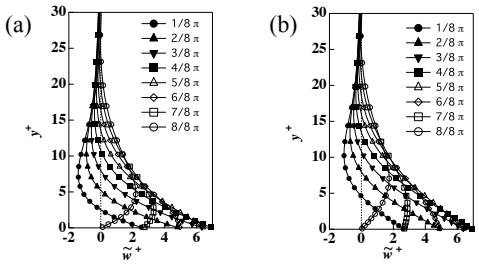

Fig. 8 Phase fluctuation parts of $\tilde{w}$. (a) temporally-periodic control, (b) spatially-periodic control.

Fukagata *et al*. (2001) shows that, for fully developed channel flow, the friction drag coefficient C_f is represented as an integral equation with Reynolds stress $-\overline{u'v'}$:

$$C_f = \frac{12}{\mathrm{Re}_b} + 12\int_{2\delta} (1-y)(-\overline{u'v'})dy. \tag{10}$$

Eq. (10) is normalized by the doubled bulk velocity $2U_b$ and the channel half-width δ. This equation means that suppression of Reynolds stress near the wall is primarily important. Reynolds stress can be decomposed by Eq. (8) into two parts, i.e., the phase fluctuation part $-\overline{\tilde{u}\tilde{v}}$, and the irregular incoherent part $-\overline{u''v''}$ as:

$$\begin{aligned} -\overline{u'v'} &= -\overline{\tilde{u}\tilde{v}} - \overline{\tilde{u}v''} - \overline{u''\tilde{v}} - \overline{u''v''} \\ &= -\overline{\tilde{u}\tilde{v}} - \overline{u''v''}. \end{aligned} \tag{11}$$

Fig. 9 shows contributions of the above two Reynolds stresses. It is revealed that contributions of $-\overline{\tilde{u}\tilde{v}}$ is negligibly small, and $-\overline{u''v''}$ governs the friction drag in both controls. In order to investigate the phase dependency of $-u''v''$, $-\widetilde{u''v''}$ at different phases are also plotted in Fig. 9. The phase dependency of phase fluctuations in the spatially-periodic control is larger than that in the temporally-periodic control. This is because the correlation between u'' and v'' is more sensitive to phases in the spatially-periodic control (as shown in Fig. 10).

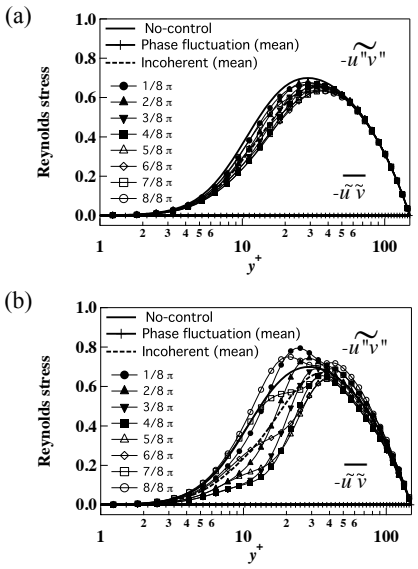

Fig. 9 Reynolds stress, phase fluctuation part $-\overline{\tilde{u}\tilde{v}}$ and incoherent part $-\overline{u''v''}$. (a) temporally-periodic control, (b) spatially-periodic control.

Quadrant Analysis

The incoherent Reynolds stress is further divided into four events depending on the signs of u'' and v''.

1. Q1 event; $u'' > 0$ and $v'' > 0$.
2. Q2 event; $u'' < 0$ and $v'' > 0$.
3. Q3 event; $u'' < 0$ and $v'' < 0$.
4. Q4 event; $u'' > 0$ and $v'' < 0$.

It is known that the above-mentioned four events are associated with a longitudinal vortex near the wall. According to Eq. (10), Q2 and Q4 events contribute to increase drag, while Q1 and Q3 decrease drag.

Fig. 9 shows the contribution of each event. The vertical axis is weighted Reynolds stress in accordance with Eq. (10). Although contributions of four events decrease in both controls, Q2 and Q4 events are reduced significantly. This suggests that the drastic decrease in Q2 and Q4 is a primary reason for drag reduction in both controls. In addition, Q2 event in the spatially-periodic control is more attenuated than that in the temporally-periodic control. This explains why the spatially-periodic control is more effective in reducing drag than the temporally-periodic control.

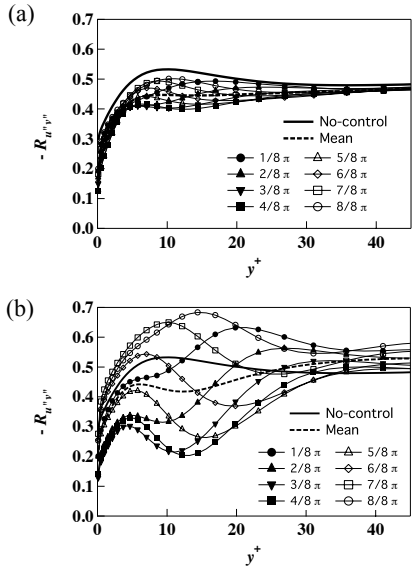

Fig. 10 Correlation between u'' and v''. (a) temporally-periodic control, (b) spatially-periodic control.

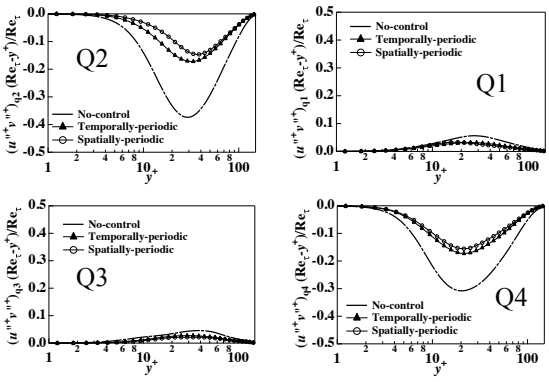

Fig. 11 Quadrant contribution of the incoherent Reynolds stress $-u''v''$.

Conditional Sampling

In order to explain the phase-dependency of $-\widetilde{u''v''}$ as shown in Fig. 9, and also drastic decrease of Q2 and Q4 events in controlled flows shown in Fig. 11, we calculate the two dimensional conditional average of the flow field around the longitudinal vortex in the flow cross sectional plane. First we capture points where the longitudinal vortex exists by detecting the point where the second invariant Q^+ of deformation tensor is lower than - 0.02 within y^+ = 10 - 20. Among these selected points, we define vortex cores (c_z, c_y), where the local pressure becomes minimum. Since the response of the longitudinal vortex to wall displacement in a particular direction should depend on the rotational direction

of the longitudinal vortex, we only choose vortex cores with $\omega_x > 0$. Then, we average the velocity field around the core for $\Delta z^+ = z^+ - c_z = -40 \sim 40$ in the spanwise direction, and $y^+ = 0 \sim 40$ in the normal direction.

Fig. 10 shows the number of detected vortex cores. The horizontal axis is phase number n, which represents the phase of $n/8\pi$. Total number of vortices is increased by 59% than that of no-controlled in the temporally-periodic control, and it is decreased by 5.35% in the spatially-periodic control. Especially, the number of vortices at $2/8\pi \sim 7/8\pi$ is decreased in both controls. In addition, this trend is more prominent in the spatially-periodic control. If we detect negative vortex cores, the number of detected vortices is decreased at $10/8\pi \sim 15/8\pi$, and increased at $2/8\pi \sim 7/8\pi$. It is assumed that the phase-dependency of $-u''v''$ is caused by changes in the number of longitudinal vortices at each phase.

Fig. 11 shows conditionally sampled flow structures. Contours show u''; solid, and dotted lines denote positive and negative values, respectively. The positional relationship of the low-speed streak and the longitudinal vortex is drastically changed at each phase. This trend agrees well with that reported by Choi *et al*. (2002) for spanwise wall-oscillation control. We consider these positional changes are the main reason for the reduction of $-u''v''$. At $1/8\pi \sim 7/8\pi$, spanwise wall velocity is positive, and therefore opposes to the vortex motion above the wall. As a result, the low-speed streak region is disappeared, so that Q2 event is reduced. At $10/8\pi \sim 16/8\pi$, spanwise wall velocity becomes negative, and high-speed region is dragged below the vortex. As the same time, the low-speed streak is pushed up above the vortex. Then, Q2 event migrates far from the wall. In summary, Q2 event is always reduced regardless of the direction of wall displacement.

CONCLUSIONS

We investigated effects of temporally- and spatially-periodic spanwise control input on near-wall coherent structures and the resultant drag reduction. As a result, we obtained the following conclusions:

1. Spatially-periodic control achieves better performance than temporally-periodic control. The spatially-periodic control can get higher drag reduction rate DR than temporally-periodic control at the same power input. The gain G and the energy saving rate S are generally higher in the spatially-periodic control than those in the temporally-periodic control.
2. In both temporally- and spatially-periodic controls, there exist the optimal time period of $T^+ \sim 100$ and wavelength $\lambda_x^+ \sim 1000$, in terms of drag reduction. Taking into account the typical convection velocity of coherent structures near the wall, the above optimal wavelength $\lambda_x^+ \sim 1000$ coincides with the optimal time period. This suggests that the spanwise fluctuation of $T^+ \sim 100$ is effective to diminish the active coherent structures near the wall.
3. By decomposing Reynolds stress into a phase fluctuation part and an incoherent part, it is found that the incoherent part is dominant in both temporally- and spatially-periodic controls. The incoherent part of the Reynolds stress tends to diminish when the wall velocity amplitude reaches its maximum value. In addition, this phase-dependency is more significant in the spatially-periodic control.
4. A conditionally-averaged flow field shows that a low-speed streak associated with the longitudinal vortex is drastically damped at the wall regardless of the direction of wall displacement. This decreases Q2 event near the wall, and therefore reduce frictional drag.

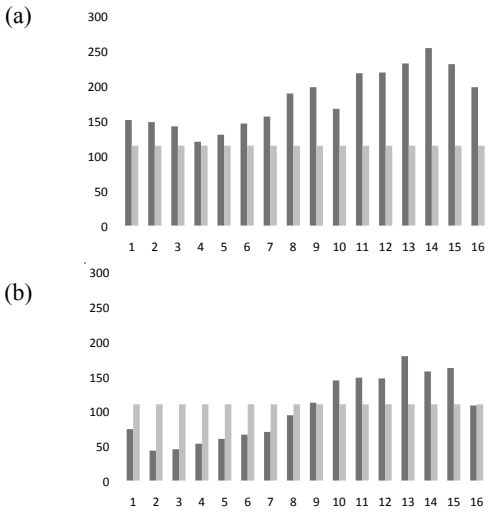

Fig. 12 The rate of detected vortex number; gray bar is no-controlled, black bar is controlled. (a) temporally-periodic control. (b) spatially-periodic control.

REFERENCES

Choi, J-. I., Xu, C-. X. and Sung, H. J., 2002, "Drag reduction by spanwise wall oscillation in wall-bounded turbulence flows," AIAA Journal, Vol. 40, No. 5, pp. 842-850.

Du, Y., and Karniadakis, G. E., 2000, "Suppressing wall-turbulence via a transverse traveling wave", Science, Vol. 288, pp. 1230-1234.

Filippone, A., 2000, "Data and performances of selected aircraft and rotorcraft", Progress in Aerospace Science, Vol. 36, pp. 629-654.

Fukagata, K., Iwamoto, K. and Kasagi, N., 2002, "Contribution of Reynolds stress distribution to the skin friction in wall-bounded flows," Phys. of Fluids, Vol. 14, L73-L76.

Jimenez, J. and Moin, P., 1991, "The minimal flow unit in near-wall turbulence," J. Fluid Mech., Vol. 225, pp. 213-240.

Jung, W., J., Mangiavacchi, N. and Akhavan, R., 1992, "Suppression of turbulence in wall-bounded floes by high frequency spanwise oscillations", Phys. Fluids A, Vol. 6, pp. 335-359.

Kawahara, G. and Kida, S, 2001, "Periodic motion embedded in plane Couette turbulence: regeneration cycle and burst," J. Fluid Mech., Vol. 449, pp. 291-300.

Quadrio, M., and Ricco, P., 2004, "Critical assessment of turbulent drag reduction through spanwise wall oscillations", J. Fluid Mech., Vol. 521, pp. 251-271.

Tardu, S., 1998, "Near wall turbulence control by local time periodical blowing," Experimental Thermal and Fluid Science, Vol. 16, pp. 41-53.

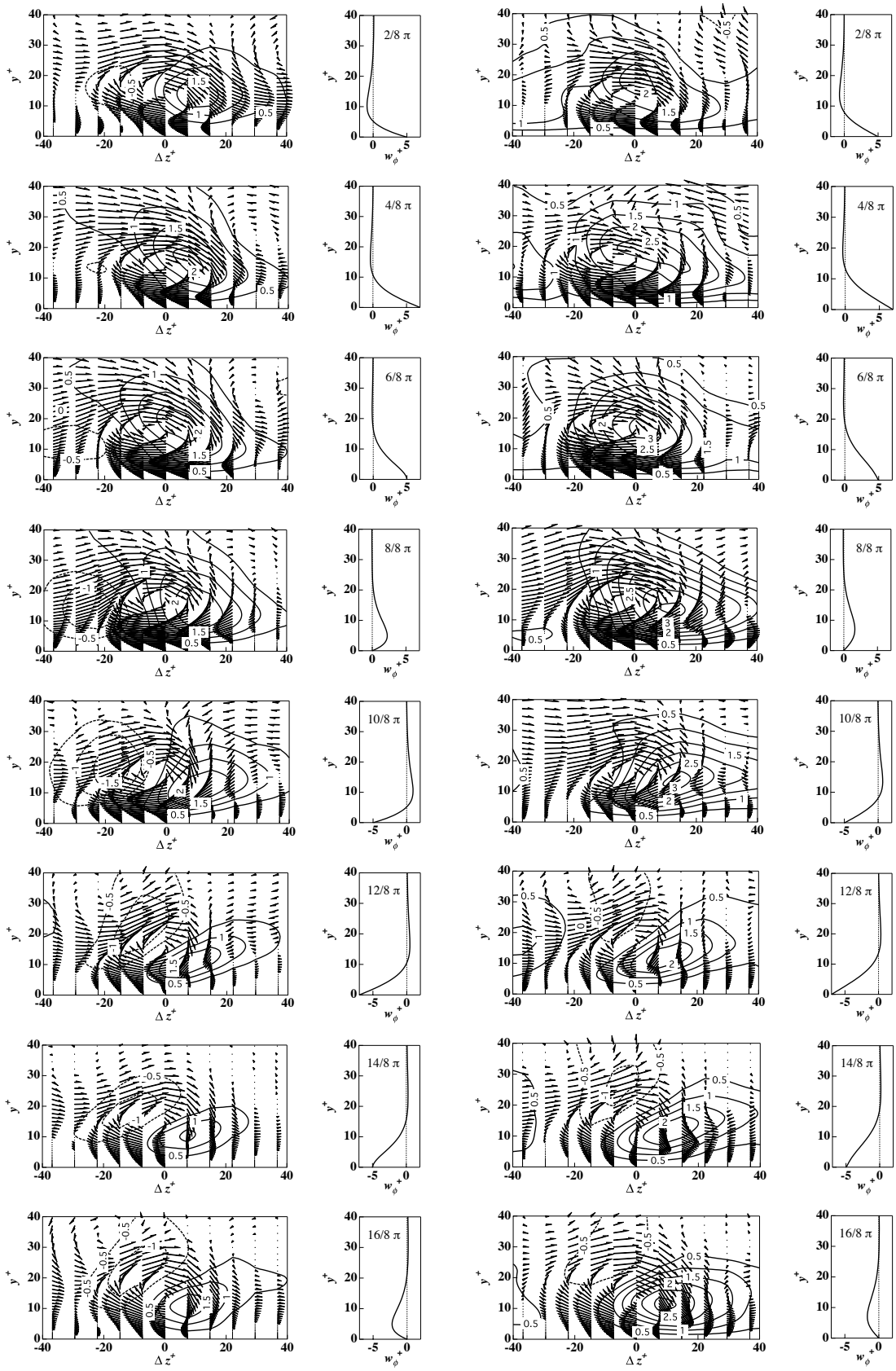

Fig. 13 Conditionally-sampled flow structures, when $\omega_x > 0$. Left is temporally-periodic control, and right is spatially-periodic control.